

Cell Reports, Volume 20

Supplemental Information

Alternative Splicing of P/Q-Type Ca²⁺ Channels

Shapes Presynaptic Plasticity

Agnes Thalhammer, Andrea Contestabile, Yaroslav S. Ermolyuk, Teclise Ng, Kirill E. Volynski, Tuck Wah Soong, Yukiko Goda, and Lorenzo A. Cingolani

This file includes:

SUPPLEMENTAL FIGURES

- Figure S1. Exogenous Ca_v2.1[EFa] and Ca_v2.1[EFb] are targeted to axons and presynaptic boutons.
- Figure S2. Exogenous Ca_v2.1[EFa] and Ca_v2.1[EFb] partially replace endogenous Ca_v2.1 channels.
- Figure S3. Exogenous Ca_v2.1[EFa] and Ca_v2.1[EFb] boost presynaptic Ca²⁺ signals.
- Figure S4. Further characterization of the knockdown of Ca_v2.1[EFa] and Ca_v2.1[EFb].
- Figure S5. Further optogenetic characterization in acute brain slices of the *in vivo* knockdown of Ca_v2.1[EFa] and Ca_v2.1[EFb].
- Figure S6. Relationship between synaptotagmin uptake and Ca_v2.1 expression at individual boutons.
- Figure S7. Working model for Ca_v2.1[EFa] and Ca_v2.1[EFb] configuration at hippocampal synapses.

SUPPLEMENTAL EXPERIMENTAL PROCEDURES

DNA constructs

RNA interference

Real Time quantitative PCR (RT-qPCR)

AAV production and stereotactic injections

Electrophysiology in primary cultures

Electrophysiology and optogenetics in acute brain slices

Presynaptic Ca²⁺ imaging with SyGCaMP3 and SyGCaMP6s

Presynaptic Ca²⁺ imaging with Fluo-4

Imaging of vesicle cycling with synaptophysin-pHluorin

Synaptotagmin antibody live uptake and confocal microscopy

Statistical analysis

SUPPLEMENTAL REFERENCES

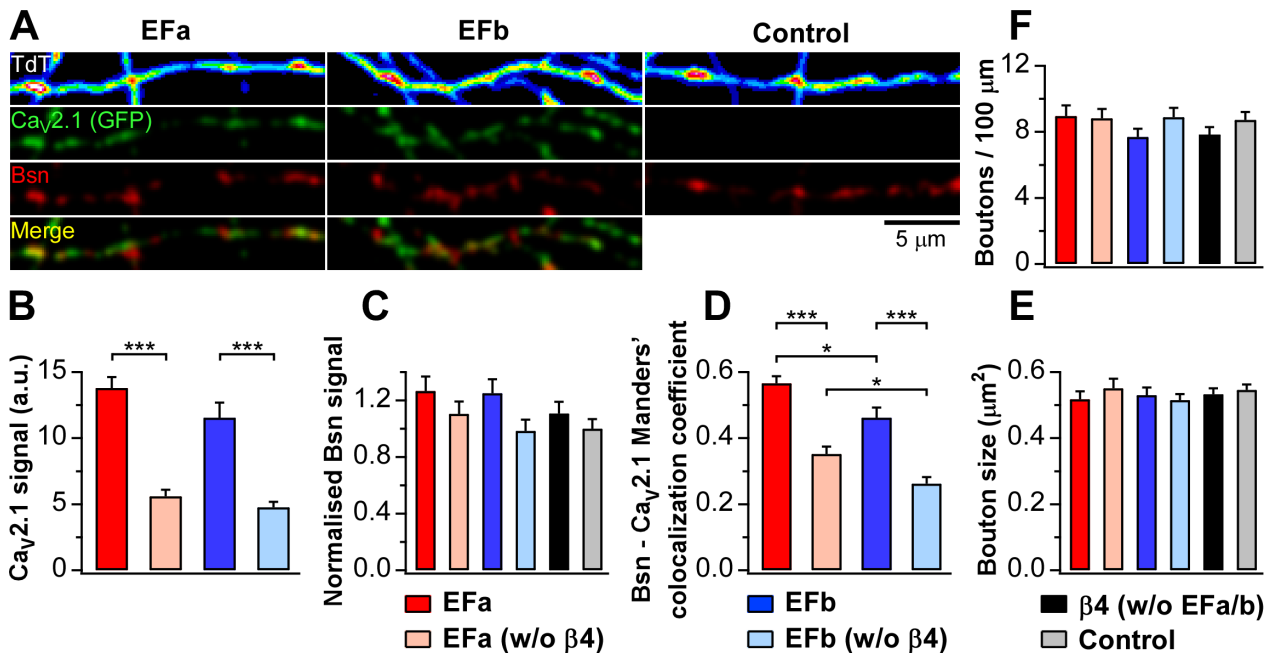


Figure S1. Exogenous Ca_v2.1[EFa] and Ca_v2.1[EFb] are targeted to axons and presynaptic boutons. Related to figures 1, 2 and 3. **(A)** Confocal microscopy images of primary hippocampal axons expressing Ca_v2.1[EFa] (EFa; left panels) or Ca_v2.1[EFb] (EFb; middle panels) tagged with EGFP at the N-terminus, together with the auxiliary subunit β4 and TdTomato. In Control (right panel), only TdTomato was expressed. Bassoon (Bsn) and TdTomato (TdT) were used as presynaptic and morphological markers, respectively. Both splice isoforms are targeted to axons and presynaptic boutons. **(B)** Quantification of Ca_v2.1[EFa] and Ca_v2.1[EFb] expression levels for experiments as in (A), showing the requirement of the auxiliary subunit β4 for effective expression and axonal targeting of Ca_v2.1[EFa] and Ca_v2.1[EFb]. **(C)** Quantification of the effects of exogenous constructs on bassoon expression level. Data are normalized to controls. **(D)** The Manders' co-localization coefficient for bassoon with Ca_v2.1 in the four experimental conditions considered. The co-localization of bassoon with Ca_v2.1[EFa] is ~20% higher than that with Ca_v2.1[EFb]. Co-expression of β4 increases the Manders' coefficient for both splice isoforms without affecting their relative differences (n = 40, 40, 41, 40, 44 and 42 fields of view for EFa, EFa (w/o β4), EFb, EFb (w/o β4), β4 (w/o EFa/b) and Control, respectively; *p<0.05 and ***p<0.001). **(E, F)** Quantification of the effects of exogenous constructs on bouton size (E) and number (F). Data are presented as mean±SEM.

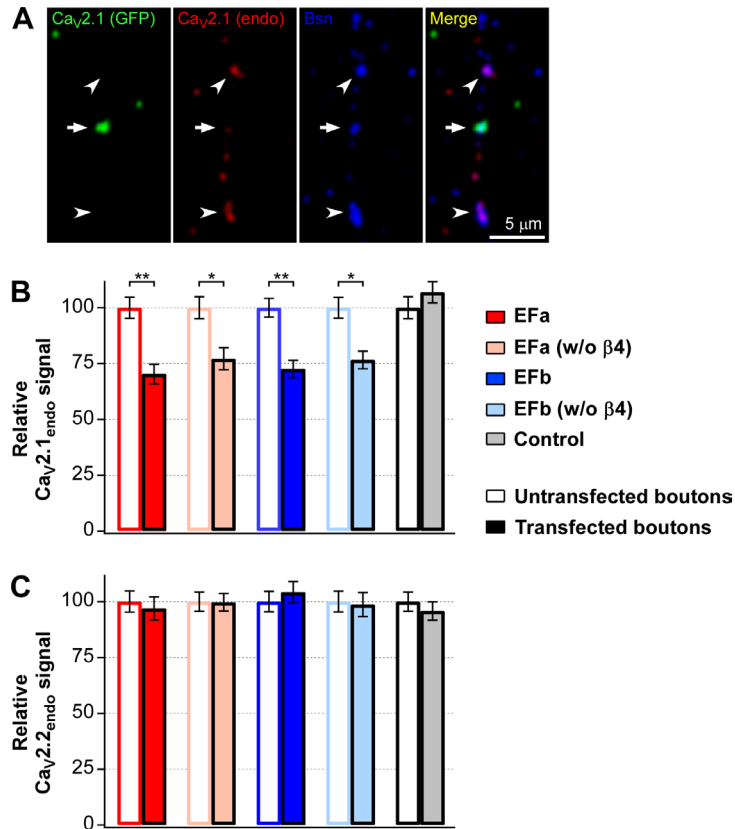


Figure S2. Exogenous Ca_v2.1[EFa] and Ca_v2.1[EFb] partially replace endogenous Ca_v2.1 channels. Related to figures 1, 2 and 3. **(A)** Primary hippocampal neurons were sparsely transfected with human Ca_v2.1[EFb] tagged with EGFP at the N-terminus and the auxiliary subunit β4. Confocal microscopy was used to co-label exogenous human Ca_v2.1 channels, via the EGFP tag (green), endogenous Ca_v2.1 channels (red), using an antibody specific for rodent Ca_v2.1 channels (Schneider et al., 2015), and the presynaptic marker bassoon (Bsn, blue). The expression level of endogenous Ca_v2.1 channels is reduced in transfected boutons (arrows) as compared to nearby untransfected boutons (arrow heads). **(B)** Quantification for experiment as in (A). In Control only EGFP was expressed. Expression of exogenous Ca_v2.1[EFa] or Ca_v2.1[EFb], with or without co-expression of the auxiliary subunit β4, reduces the expression level of endogenous P/Q-type Ca_v2.1 channels (n = 100 boutons for each condition; *p≤0.04, **p≤0.007). **(C)** As in (B) but for endogenous N-type Ca_v2.2 channels. Expression of exogenous Ca_v2.1 splice isoforms does not significantly affect the expression level of endogenous Ca_v2.2 channels (n = 100 boutons for each condition). Data are presented as mean±SEM.

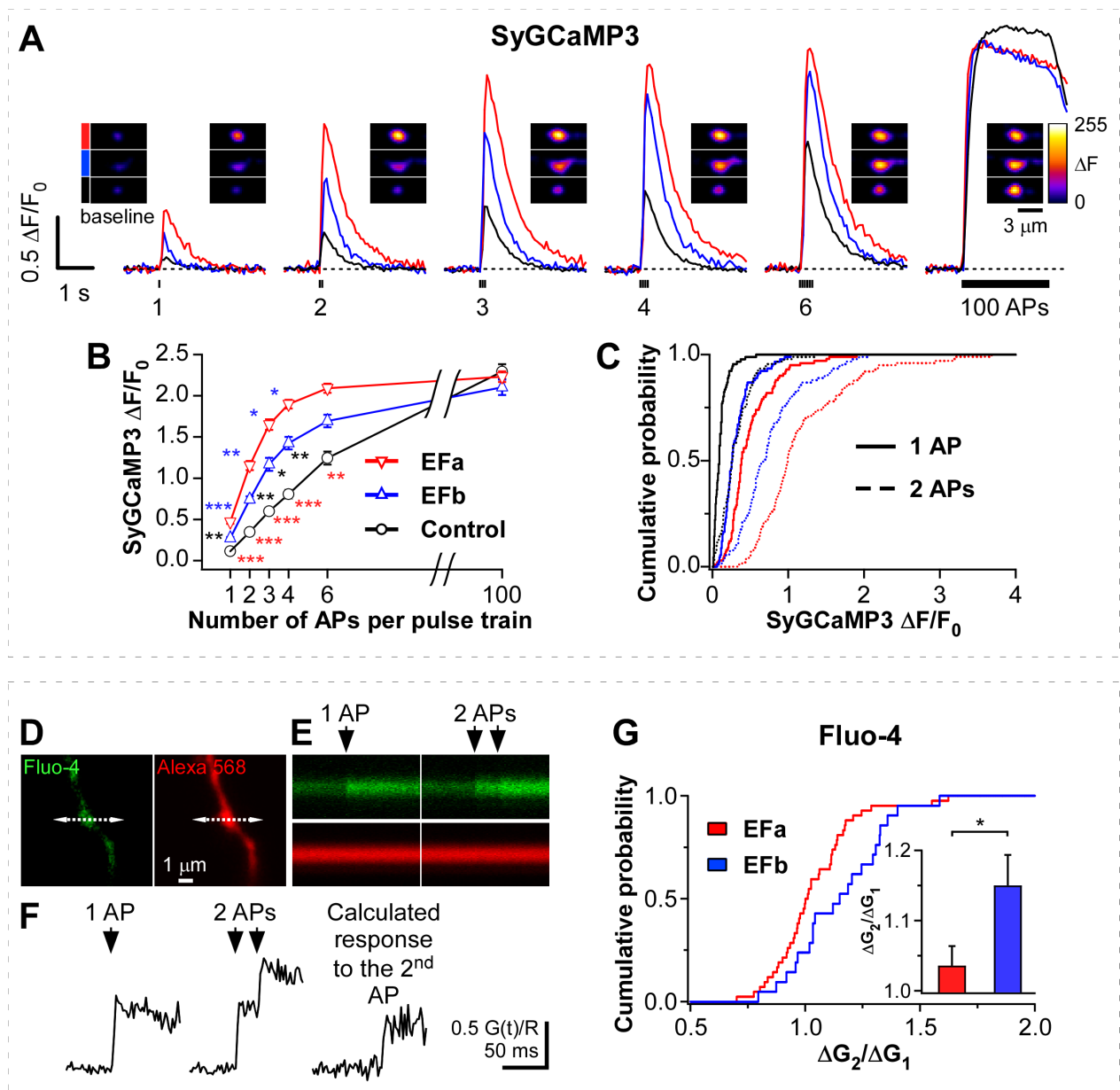


Figure S3. Exogenous $Ca_v2.1[EFa]$ and $Ca_v2.1[EFb]$ boost presynaptic Ca^{2+} signals. Related to figures 1, 2 and 3. **(A-C)** Imaging presynaptic Ca^{2+} transients with SyGCaMP3 in primary hippocampal cultures. **(A)** SyGCaMP3 responses from representative experiments. Traces show averages of 31, 15 and 18 boutons from individual fields of view for $Ca_v2.1[EFa]$ (red), $Ca_v2.1[EFb]$ (blue) and Control (black; boutons without expression of exogenous $Ca_v2.1$ channels) in response to the indicated number of APs delivered at 40Hz. Inset, individual boutons for the three conditions. **(B)** Average peak amplitude of SyGCaMP3 for experiments as in (A) ($n=7$, 8 and 8 independent experiments for $Ca_v2.1[EFa]$, $Ca_v2.1[EFb]$ and Control, respectively; $*p<0.05$, $**p<0.01$ and $***p<0.001$). **(C)** Cumulative distribution of individual boutons in response to one (continuous lines) and two (dotted lines) APs for $Ca_v2.1[EFa]$ ($n=100$), $Ca_v2.1[EFb]$ ($n=91$) and Control ($n=91$). $Ca_v2.1[EFa]$ is more efficient than $Ca_v2.1[EFb]$ in increasing SyGCaMP3 signals. **(D-F)** Typical experiment for imaging presynaptic Ca^{2+} dynamics with Fluo-4 in primary hippocampal cultures. **(D)** Images of a presynaptic bouton and axonal fragment of a $Ca_v2.1[EFa]$ neuron (left, Fluo-4 channel; right, Alexa 568 channel; dotted lines indicate positions of the line-scan for recording fast AP-evoked Ca^{2+} dynamics). **(E)** Fluorescence responses to single (left) and paired (25 ms interval; right) APs in the bouton from (D). Top, Fluo-4 channel; bottom, Alexa 568 channel. Images are averages of five sweeps. **(F)** Fluo-4 responses to one (left) and two APs (middle) normalized to Alexa568 fluorescence ($G(t)/R$) from (E). Right, digitally calculated response to the second AP. **(G)** Ratio of the fluorescence responses between the second and first AP ($\Delta G_2/\Delta G_1$) for individual boutons ($n = 42$ and 21 for $Ca_v2.1[EFa]$ and $Ca_v2.1[EFb]$, respectively) for experiments as in (D-F). Inset, bar graph summary of the same data. $Ca_v2.1[EFb]$ induces a small paired-pulse facilitation of presynaptic Ca^{2+} signals ($*p=0.03$). Data are presented as mean \pm SEM.

Figure S4. Further characterization of the knockdown of Ca_v2.1[EFa] and Ca_v2.1[EFb]. Related to figures 4, 5 and 6. **(A)** Evaluation of the knockdown efficiency and selectivity of isoform-specific microRNAs (miRs) for Ca_v2.1[EFa] and Ca_v2.1[EFb]. Isoform-specific RT-qPCR analysis on RNA isolated from 17-18 DIV primary cultures infected at 6 DIV with adeno-associated viruses (AAVs) expressing miRs targeting either Ca_v2.1[EFa] (miR EFa1 and miR EFa3) or Ca_v2.1[EFb] (miR EFb2). Data are normalized to the negative control (miR Control). miR EFa1 and miR EFa3 significantly reduce mRNA of Ca_v2.1[EFa] (by ~70%; n = 8 and 7 cultures) but not that of Ca_v2.1[EFb], whilst miR EFb significantly reduces mRNA of Ca_v2.1[EFb] (by ~60%; n = 4 cultures; ***p<0.001) but not that of Ca_v2.1[EFa]. For detailed information on the knockdown strategy refer to supplemental experimental procedures. **(B)** Typical experiment for imaging vesicle release with SybHy in primary hippocampal cultures following transfection with isoform-specific miRs for Ca_v2.1[EFa] and Ca_v2.1[EFb]. SybHy responses for miR Control to 40 APs delivered at 20 Hz before and after EGTA-AM application (200 μM, loaded for 90 s, followed by 10 min wash), and following rapid alkalization of the entire vesicle pool with NH₄Cl (50 mM), as indicated. **(C)** Summary of experiments as in (B) (n=10, 13, 12 and 11 independent experiments for miR Control, miR EFa1, miR EFa3 and miR EFb2, respectively). Knockdown of either Ca_v2.1[EFa] or Ca_v2.1[EFb] has no effect on the pre-EGTA responses normalized to the total vesicle pool size at each bouton. **(D-F)** Imaging presynaptic Ca²⁺ transients with SyGCaMP6s in primary hippocampal cultures. Presynaptic Ca²⁺ transients are largely reduced by knockdown of either Ca_v2.1[EFa] or Ca_v2.1[EFb], and severely compromised when both splice isoforms are targeted. SyGCaMP6s recordings were performed in the presence of ω-conotoxin GVIA (1 μM) to block N-type Ca²⁺ channels and measure the contribution of P/Q-type Ca_v2.1[EFa] and Ca_v2.1[EFb] isoforms to presynaptic Ca²⁺ in relative isolation (see supplemental methods). **(D)** SyGCaMP6s responses from representative experiments. Traces are averages of 17, 20, 19 and 12 boutons from individual fields of view for miR Control (black), miR EFa1 (red), miR EFb2 (blue) and miR EFa1 + miR EFb2 (green) in response to the indicated number of APs delivered at 40 Hz. Inset, higher magnification for one and two APs. **(E)** Average peak amplitude of SyGCaMP6s for experiments as in (D) (n=18, 14, 9, 16 and 14 independent experiments for miR Control, miR EFa1, miR EFa3 (orange), miR EFb2 and miR EFa1 + miR EFb2, respectively; *p<0.05, **p<0.01 and ***p<0.001. Inset, higher magnification for one and two APs. **(F)** Cumulative distribution of ΔF/F₀ for individual boutons in response to one (left) and two (right) APs (n=263, 231, 96, 213 and 203 boutons for miR Control, miR EFa1, miR EFa3, miR EFb2 and miR EFa1+EFb2, respectively). Data are presented as mean±SEM.

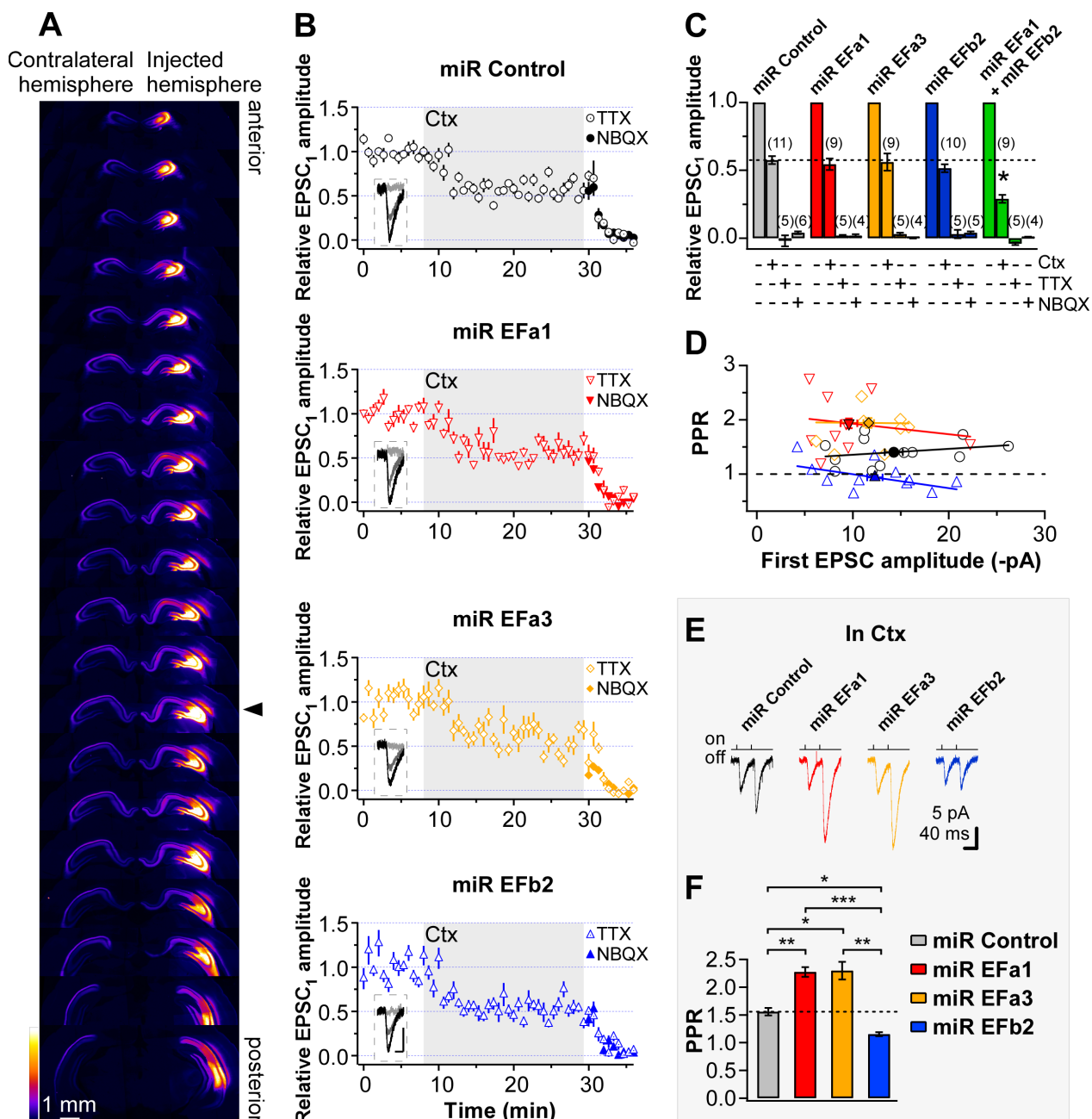


Figure S5. Further optogenetic characterization in acute brain slices of the *in vivo* knockdown of Ca_v2.1[Efa] and Ca_v2.1[Efb]. Related to figure 6. **(A)** Serial coronal sections of rat brain aligned along the anterior-posterior axis. AAV, expressing miR Control and the ultrafast channelrhodopsin ChETA fused to TdTomato, was stereotactically injected into the CA3 region of the right hippocampus at the indicated location (arrowhead). TdTomato fluorescence is visible in the CA3 region and in CA3 ipsi- and contra-lateral axonal projections along the anterior-posterior axis. Optogenetic experiments were done with bilateral injections. **(B, C)** Acute application of ω-conotoxin GVIA (1 μM; Ctx) induces a ~42% reduction of the amplitude of optogenetically evoked EPSCs under control conditions (miR Control), similarly to the previously reported effect of Ctx on electrically evoked EPSCs at these synapses (Reid et al., 1998; Scheuber et al., 2004; Scholz and Miller, 1995; Wu and Saggau, 1994). miR Efa1, miR Efa3 and miR Efb2 do not significantly change this percentage, arguing against a compensatory up-regulation of N-type Ca²⁺ channels upon knockdown of one P/Q-type Ca²⁺ channel splice isoform. When both isoforms are knocked down (miR Efa1 + miR Efb2), the Ctx-dependent reduction of EPSCs is significantly larger than in control conditions (~71%; *p<0.05 relative to miR Control; green scale bars in (C)). Optogenetically evoked EPSCs are completely blocked by TTX or NBQX, indicating that they are AP-dependent and mediated by AMPARs. Insets in (B), representative EPSC traces under basal conditions (Black), after Ctx (dark grey) and TTX (in miR Efa1 and miR Efb2) or NBQX (in miR Control and miR Efa3) application (light gray); scale bars 5 pA and 20 ms. In (C), numbers of recorded cells are indicated in brackets; dashed line refers to the amplitude of EPSCs with Ctx in the miR Control group. **(D)** PPR vs. amplitude of first EPSC during baseline, showing that the differences in PPR are not

secondary to differences in the amplitude of the first EPSC. Lines are linear regression fits. Open symbols represent individual recordings, filled symbols population averages. Stimulation strength was adjusted to yield small EPSCs (<30 pA). **(E, F)** As in (D, E) of figure 6 but after application of Ctx. The increase in PPR with miR EFa1 and miR EFa3 and its decrease with miR EFb2, relative to miR Control, are maintained after blockade of N-type Ca²⁺ channels (*p<0.05; **p<0.005; ***p<0.0001), suggesting that the differences in PPR result from a shift in Ca_v2.1 splice isoform composition. Data are presented as mean±SEM.

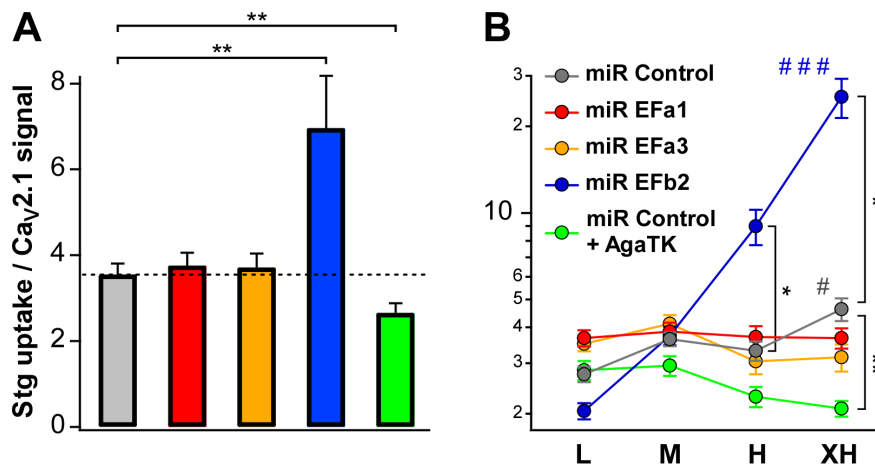


Figure S6. Relationship between synaptotagmin uptake and Ca_v2.1 expression at individual boutons. Related to figure 7. **(A)** The ratio between synaptotagmin (Stg) uptake level and Ca_v2.1 fluorescence signal at individual boutons was taken as measure of presynaptic efficacy of Ca_v2.1. Relative to controls (miR Control), synaptic efficacy is largely increased by knockdown of Ca_v2.1[EFb] (miR Efb2), unchanged by knockdown of Ca_v2.1[Efa] (miR Efa1 and miR Efa3) and reduced by pharmacological blockade of Ca_v2.1 channels with ω-agatoxin TK (300 nM; miR Control + AgaTK; **p≤0.009; n = 497, 194, 248, 244 and 232 boutons for miR Control, miR Efa1, miR Efa3, miR Efb2 and miR Control + AgaTK, respectively). **(B)** Boutons were divided into four groups of increasing Stg fluorescent signal (L = low activity, M = medium activity, H = high activity, XH = extra high activity, corresponding to a Stg fluorescent signal of 0-10, 10-20, 20-30 and >30 a.u., respectively), and the average of the ratio between Stg uptake level and Ca_v2.1 signal at individual boutons was plotted for each group. In control conditions (miR Control), presynaptic efficacy of Ca_v2.1 is moderately higher in more active boutons (# p=0.03). Knockdown of Ca_v2.1[EFb] largely increases this correlation (miR Efb2; ### p<0.0001), whereas knockdown of Ca_v2.1[Efa] (miR Efa1 and miR Efa3) or pharmacological blockade of Ca_v2.1 with ω-agatoxin TK (300 nM; miR Control + AgaTK) abolishes it. Statistical analyses within each of the four groups of increasing activity levels reveal that synaptic efficacy is higher for miR Efb2 in the H and XH groups (*p≤0.03), and smaller for miR Control + AgaTK in the XH group (**p=0.005), relative to miR Control. Same data set as in figure 7B-E. Data are presented as mean±SEM. The relationship between Stg uptake and Ca_v2.1 expression at individual boutons in the presence of Ca_v2.1 isoform-specific miRs suggests that (i) endogenous Ca_v2.1[Efa] (miR Efb2 condition) is overall more efficient than endogenous Ca_v2.1[EFb] (miR Efa1 and miR Efa3 conditions) in supporting Stg uptake and that (ii) the efficiency of endogenous Ca_v2.1[Efa] is higher at more active boutons, while that of Ca_v2.1[EFb] is independent of the activity level of the boutons.

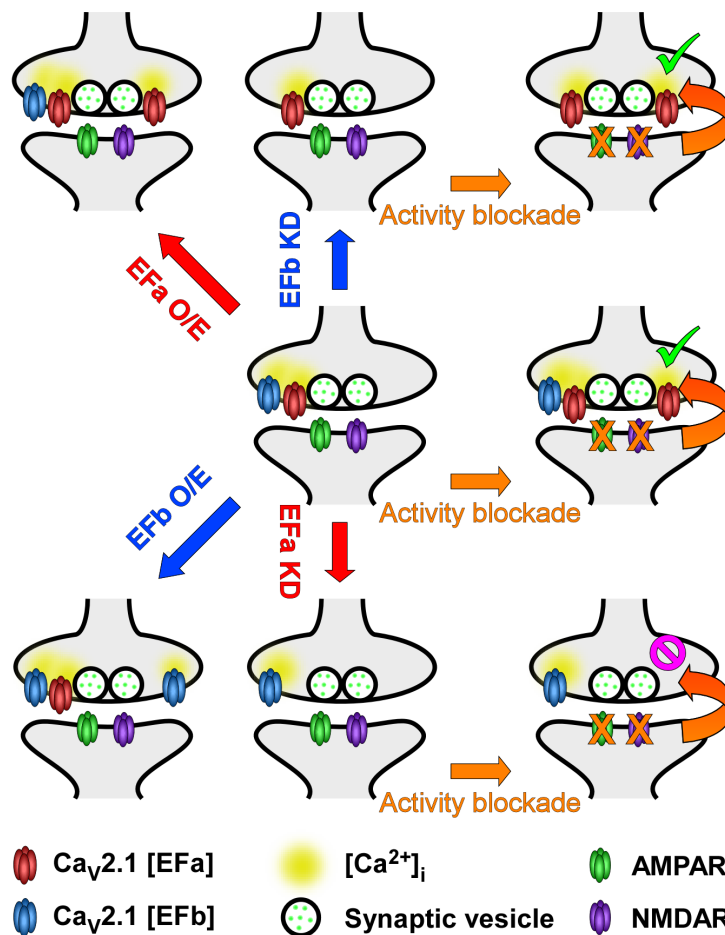


Figure S7. Working model for $\text{Ca}_v2.1[\text{EFa}]$ and $\text{Ca}_v2.1[\text{EFb}]$ configuration at hippocampal synapses. Related to all figures. Over-expression of $\text{Ca}_v2.1[\text{EFa}]$ (top left) favors tight coupling between $\text{Ca}_v2.1$ channels and synaptic vesicles at most synapses (figure 3), resulting in high P_r (figure 1G and 2) and PPD (figure 1D-F). Over-expression of $\text{Ca}_v2.1[\text{EFb}]$ (bottom left) favors loose coupling at many synapses (figure 3), thus promoting lower P_r (figure 1G and 2) and PPF (figure 1D-F). Knockdown of $\text{Ca}_v2.1[\text{EFb}]$ (top center) leaves in place $\text{Ca}_v2.1[\text{EFa}]$ channels, which display high synaptic efficacy (figure S6) and are less sensitive to EGTA (figure 5); this results in decreased PPR (figure 6). In top right, blockade of postsynaptic AMPA and NMDA receptors activates retrograde signals that lead to presynaptic homeostatic plasticity, involving an increase in vesicle number (not depicted; (Thalhammer and Cingolani, 2014)) and insertion of $\text{Ca}_v2.1[\text{EFa}]$ channels (figure 7B-E), as for naïve boutons (middle left; figure 7B-E). Knockdown of $\text{Ca}_v2.1[\text{EFa}]$ (bottom center) leaves in place $\text{Ca}_v2.1[\text{EFb}]$ channels, which display low synaptic efficacy (figure S6) and are more sensitive to EGTA (figure 5); this results in increased PPR (figure 6). In bottom right, blockade of postsynaptic AMPA and NMDA receptors fails to induce presynaptic homeostatic plasticity because $\text{Ca}_v2.1[\text{EFa}]$ channels for insertion are lacking (figure 7B-E). As for previously proposed models of P/Q-type and N-type Ca^{2+} channels (Cao et al., 2004; Cao and Tsien, 2010), this model assumes that there are P/Q-type channel isoform-specific slots in the presynaptic membrane, with $\text{Ca}_v2.1[\text{EFa}]$ and $\text{Ca}_v2.1[\text{EFb}]$ channels not interchangeable. Drawing is not to scale; numbers of channels and vesicles are not intended to be quantitative.

Supplemental Experimental Procedures

DNA constructs

For experiments in primary cultures, we used human Ca_v2.1[Δ10A (+G), 16+/17+, Δ17A (-VEA), +31* (+NP), 37a (EFa), 43+/44+, Δ47] and Ca_v2.1[Δ10A (+G), 16+/17+, Δ17A (-VEA), +31* (+NP), 37b (EFb), 43+/44+, Δ47], referred to as Ca_v2.1[EFa] and Ca_v2.1[EFb], respectively (Chaudhuri et al., 2004) (**figure 1B**). For testing microRNA (miR) efficiency in cell lines, we used rat Ca_v2.1[EFa] and Ca_v2.1[EFb] (Bourinet et al., 1999). In both cases, we co-transfected the Ca²⁺ channel auxiliary subunit β4 because it favors surface delivery of primary α_{1A} subunits without affecting morphology and number of presynaptic boutons, Ca²⁺ transients or synaptic transmission *per se* (**figure S1B-F** and (Hoppa et al., 2012; Qian and Noebels, 2000).

SyGCaMP3, in which GCaMP3 is fused to the cytoplasmic C-terminus of the synaptic vesicle protein synaptophysin, was kindly provided by Dr. Susan Voglmaier (Li et al., 2011; Niwa et al., 1991). SyGCaMP6s was cloned by swapping GCaMP3 with GCaMP6s (#40753, Addgene) (Chen et al., 2013). SyGCaMP constructs localize to synaptic vesicles, thus sampling Ca²⁺ specifically at presynaptic terminals (Dreosti et al., 2009; Li et al., 2011).

The constructs for adeno-associated virus (AAV) production (Syn-ChETA-TdT-miR-X; **figure 6A**) were derived from pAAV-Ef1a-FAS-ChETA-TdTomato-WPRE-pA (#37089, Addgene) (Saunders et al., 2012) by exchanging the Ef-1a promoter with the short human Synapsin promoter and by cloning the miR cassette from pcDNA6.2-GW/EmGFP-miR vector (K4936-00, Invitrogen) between the stop codon of ChETA-TdTomato and WPRE using the NheI and EcoRI sites. For knockdown experiments in culture ChETA was removed from Syn-ChETA-TdT-miR-X to obtain Syn-TdT-miR-X. Constructs were generated by standard cloning strategies and verified by sequencing. All constructs are available upon request.

RNA interference

mRNA target sequences for rat Ca_v2.1[EFa] and Ca_v2.1[EFb] used to design artificial microRNAs (miRs) for RNA interferences (RNAi) were selected with a dedicated software (BLOCK-iT RNAi Designer; Invitrogen; <https://rnaidesigner.lifetechnologies.com/rnaiexpress/design.do>). The miR sequences were cloned into the pcDNA6.2-GW/EmGFP-miR vector using the BLOCK-iT Pol II miR RNAi Expression Vector kit (K4936-00; Invitrogen), according to the manufacturer's instructions, thereby creating an expression cassette consisting of a 5' miR flanking region, a specific miR sequence and a 3' miR flanking region that can be expressed from the 3' UTR of a reporter gene under the control of a RNA polymerase type II promoter. As a negative control (miR Control), we used the pcDNA6.2-GW/EmGFP-miR-neg plasmid from the kit containing a sequence that does not target any known vertebrate gene. Despite the short size (97 bp) and high similarity (61.86% identity at the nucleotide level) between exons 37a and 37b, we could design three miR sequences against rat Ca_v2.1[EFa] (miR EFa1: TCCTTATAGTGAATGCGGCCG; miR EFa2: ATGTCCTTATAGTGAATGCGG; miR EFa3: TTGCAAGCAACCCTATGAGGA) and two against rat Ca_v2.1[EFb] (miR Efb1: ATACATGTCCGGGTAAGGCAT; miR Efb2: ATCTGATACATGTCCGGGTAA) with predicted high knockdown efficiency. Sequences given are antisense target sequences. Positions (in bp) relative to exons 37a/b are: 1-21 for miR EFa1; 4-24 for miR EFa2; 76-96 for miR EFa3; 8-28 for miR Efb1; 13-33 for miR Efb2. Numbers of mismatches relative to the corresponding sequence on the non-targeted exon are 8, 7, 8, 7 and 9 for miR EFa1, miR EFa2, miR EFa3, miR Efb1 and miR Efb2, respectively.

The knockdown efficiency of the five selected miRs was first evaluated by co-transfecting HEK293 cells with either rat Ca_v2.1[EFa] or Ca_v2.1[EFb] and one of the five miR vectors. Co-transfection with miR Control was used as negative control. Forty-eight hours after transfection, cells were lysed, and protein content was analyzed by immunoblot with rabbit anti-Ca_v2.1 antibody (1:2000; Cat. No. ACC-001, Alomone Labs) and rabbit anti-Actin (1:5000, Sigma). Based on this heterologous expression system, we selected two miRs against Ca_v2.1[EFa] (miR EFa1 and miR EFa3), showing 56% and 64% knockdown efficiency, respectively, and one miR against Ca_v2.1[EFb] (miR Efb2), showing 42% knockdown efficiency, to be further optimized and tested for efficiency and specificity against endogenous rat Ca_v2.1[EFa] and Ca_v2.1[EFb] using isoform-specific real time quantitative PCR (following paragraph and **figure S4A**).

Real Time quantitative PCR (RT-qPCR)

Primary rat cultures were infected at 6 DIV with AAVs expressing miR Control, miR EFa1, miR EFa3 or miR Efb2. RNA was extracted at 17-18 DIV with QIAzol reagent and purified on RNeasy spin columns (Qiagen). RNA samples were quantified with a ND1000 Nanodrop spectrophotometer (Thermo Scientific). Reverse transcription was performed with QuantiTect Reverse Transcription Kit (Qiagen). RT-qPCR was performed in triplicate with 10 ng of template cDNA using QuantiTect SYBR green master mix (Qiagen) on a 7900-HT Fast Real-time System (Applied Biosystem), as previously described (Deidda et al., 2015), with the following universal conditions: 5 min at 95 °C, 40 cycles of denaturation at 95 °C for 15 sec, and annealing/extension at 60 °C for 45 sec. Primers were designed with Beacon Designer software (Premier Biosoft) using a BLAST search in order to avoid significant cross homologies regions with other genes. For detecting Ca_v2.1[EFa] and Ca_v2.1[EFb], we used isoform-specific forward primers (EFa-fwd: 5' CTTAGGCAAGAAATGTCCTCAT 3'; Efb-fwd: 5' GGTCTTGGGAAGAAGTGC 3') and a common reverse primer (EFab-rev: 5' TTGAAGTGAACGGTGTGTC 3'). The specificity of the primers was

verified in qPCR reactions in which a plasmid containing either rat Ca_v2.1[EFa] or rat Ca_v2.1[EFb] was used as template. Product specificity and absence of primer dimers was also verified by melting curve analysis. qPCR reaction efficiency for each primer pair was calculated by the standard curve method with a four points serial dilution of cDNA. Calculated qPCR efficiency for each primer set was used for subsequent analysis. To evaluate miR efficiency and selectivity, data were normalized to glyceraldehyde-3-phosphate dehydrogenase (GAPDH; GAPDH-fwd: 5' GGTGCTGAGTATGTCGTGGA 3'; GAPDH-rev: 5' GATGATGACCCTTTTGGC 3') and β -actin (ACTB; ACTB-fwd: 5' CATCACTATCGGCAATGAGC 3'; ACTB-rev: 5' TCATGGATGCCACAGGATT 3') by the multiple internal control gene method with GeNorm algorithm (Vandesompele et al., 2002) available in qBasePlus software (Biogazelle). To evaluate activity-dependent changes in the expression of Ca_v2.1[EFa] and Ca_v2.1[EFb] (**figure 7A**), data were normalized to tubulin β 3 (TUBB3; TUBB3-fwd: 5' GCCTTTGGACACCTATTTCAG 3'; TUBB3-rev: 5' TCACATTCTTTCCTCACGAC 3') and peptidylprolyl isomerase A (PPIA; PPIA-fwd: 5' CACTGGGGAGAAAGGATTTG 3'; PPIA-rev: 5' CCATTATGGCGTGTGAAGTC 3') because the expression of these two genes displayed no statistically significant changes upon chronic activity deprivation.

In initial experiments, we noticed that the knockdown efficiency of Ca_v2.1[EFb] by miR EFb was ~50%. To increase it to values statistically equivalent to the knockdown efficiency of the other two miRs (**figure S4A**), we duplicated the miR EFb2 cassette in the 3'UTR, according to the BLOCK-iT Pol II miR RNAi Expression Vector kit's instructions, and prepared new constructs containing a double miR EFb2 cassette to be used in all subsequent tests and experiments (**figures 4-7 and S4-S6**).

For the absolute determination of Ca_v2.1[EFa] and Ca_v2.1[EFb] transcripts, standard curves prepared with serial dilutions of Ca_v2.1[EFa]- and Ca_v2.1[EFb]-containing plasmids were run in parallel to the experimental samples. RNA extracted from the CA1-CA3 region of the rat hippocampus (P40) yielded 7942±203 copy number/ng RNA (42.9±0.8%) and 10643±320 copy number/ng RNA (57.1±0.8%) for Ca_v2.1[EFa] and Ca_v2.1[EFb], respectively (n = 5 hippocampi).

AAV production and stereotactic injections

AAV1/2 expressing ChETA-TdT-miR-EFa1, ChETA-TdT-miR-EFa3, ChETA-TdT-miR-EFb2-miR-EFb2 and ChETA-TdT-miR-Control were generated as previously described (McClure et al., 2011). Briefly, HEK293T cells were co-transfected with the required AAV vector together with the plasmids pRV1, pH21 and pFdelta6 using a Ca²⁺ phosphate method. Forty-eight hrs post transfection, cells were harvested and lysed, and viruses purified over heparin columns (Ge HealthCare Life science).

Stereotactic injections were performed in P18 rats, with coordinates for CA3 of (A-P/M-L/D-V from Bregma) -2.6/± 2.9/-2.9. Expression and localization of AAVs was confirmed by TdTomato fluorescence (**figure 6B and S5A**).

Electrophysiology in primary cultures

Low density rat primary hippocampal cultures were grown on a glial feeder layer as previously described (Cingolani and Goda, 2008), transfected with Ca_v2.1[EFa] or Ca_v2.1[EFb] together with the auxiliary subunit β 4 (1:1 DNA ratio) 2-5 days prior to experiments using a Ca²⁺ phosphate method (Cingolani et al., 2008) and recorded at 12-15 days in vitro (DIV). Whole-cell paired-recordings were performed at room temperature from a transfected and a nearby untransfected pyramidal neuron. For the data reported in **figure 1**, in the case of Ca_v2.1[EFa], out of 16 connected pairs, eight expressed Ca_v2.1[EFa] in the presynaptic neuron, five in the postsynaptic one, and three displayed double connectivity; in the case of Ca_v2.1[EFb], out of 18 connected pairs, 10 expressed Ca_v2.1[EFb] in the presynaptic neuron, seven in the postsynaptic one, and one displayed double connectivity (**figure 1C**). A pair was considered not connected in one direction if no response was observed after ≥ 10 stimuli. Pairs displaying polysynaptic connectivity were discarded. AMPAR-mediated excitatory postsynaptic currents (EPSCs) were scored with a detection threshold set at two SD of the background noise over time windows of 0-8 and 8-658 ms following the end of the presynaptic Na⁺ spike for synchronous and asynchronous release, respectively.

Sister cultures were used for the two splice isoforms, and experiments were performed in parallel on at least three independent preparations. During recordings, neurons were continuously perfused with aCSF containing (in mM): 140 NaCl, 2.5 KCl, 2.2 CaCl₂, 2.3 MgCl₂, 10 D-glucose, 10 HEPES-NaOH (pH 7.38; osmolarity adjusted to 290 mOsm). A GABA_A receptor blocker (100 μ M picrotoxin) was routinely included in the aCSF. For EGTA-AM experiments, CaCl₂ was raised to 2.5 mM and MgCl₂ lowered to 1.5 mM in order to increase P_r and favor EPSC detection. To isolate NMDAR-mediated EPSCs in the MK-801 experiments, CaCl₂ and MgCl₂ were lowered to 1.5 and 0.1 mM, respectively, and aCSF was supplemented with an NMDAR co-agonist (20 μ M glycine) and an AMPAR blocker (2 μ M NBQX). The intracellular solution contained (in mM): 100 K-gluconate, 5 K-glutamate, 17 KCl, 5 NaCl, 0.5 EGTA, 5 MgCl₂, 4 K₂-ATP, 0.5 Na₃-GTP, 20 K₂-creatine phosphate, 10 HEPES-KOH (pH 7.28; osmolarity adjusted to 280 mOsm). Recordings were performed with two Axopatch 200B amplifiers (Molecular Devices). Pipette resistances were 2-3 M Ω ; series resistances were always below 20 M Ω , stable (<20% variation), not significantly different between conditions, and compensated by 70% in the postsynaptic cell. Pre- and postsynaptic neurons were voltage-clamped at -70 and -50 mV for AMPAR- and NMDAR-mediated EPSC recordings, respectively; in order to evoke synaptic transmission, unclamped Na⁺ spikes were elicited in the presynaptic neuron by delivering one or two depolarizing stimuli (+30 mV, 2 ms-long) at various interstimulus

intervals. Signals were filtered at 2 kHz, digitized at 20 kHz using Clampex 10.1 (Molecular Devices) and analyzed offline with Clampfit 10.1 (Molecular Devices) and Igor Pro 6.03 (Wavemetrics Inc.). Paired-pulse stimulations were delivered every 20 s; each paired-pulse series (10, 25, 50, 100, and 200 ms paired-pulse intervals) was repeated at least three times and averaged for each cell before calculating PPR (Kim and Alger, 2001). NMDAR-mediated EPSCs were evoked every 10 s; after a stable baseline was obtained (≥ 12 stimuli), stimulation was stopped, neurons were voltage-clamped at -70 mV and MK-801 ($5 \mu\text{M}$) was perfused for 3 min before resuming stimulation (100 stimuli) in the continuous presence of MK-801.

For overlapping EPSC pairs, the peak amplitude of the second EPSC was estimated as follows: all non-overlapping EPSCs from the same cell were averaged, the resulting mean EPSC was synchronized with and scaled to the peak of the first EPSC in the overlapping pair, and subtracted from the second EPSC; the resulting peak was taken as best amplitude estimation of the second EPSC.

To measure the coefficient of variation (CV) of the first EPSC, synaptic responses were base-lined using a 10 ms window immediately preceding the start of the EPSCs, and then averaged. A measurement window of 1 ms was placed at the peak of the averaged EPSC to measure synaptic responses. To measure the background noise, a second measurement window of 1 ms preceded the baseline in such a way that the baseline window was equidistant between the two measurement windows. CV was then calculated as $CV = \sqrt{(\sigma_p^2 - \sigma_b^2)}/\mu_p$ where μ_p is the mean of the EPSC peak, σ_p^2 the variance of the EPSC peak and σ_b^2 the variance of the background noise (Cingolani and Goda, 2008; Silver, 2003).

Synaptic latency, measured from the end of the presynaptic Na^+ spike to 5% of the EPSC amplitude (Boudkkazi et al., 2007), was not modified by EF-hand-like splice isoforms (Efa pre: 2.45 ± 0.54 ms; Efa post: 2.57 ± 0.67 ms; EFb pre: 2.84 ± 0.33 ms; EFb post: 2.49 ± 0.70 ms; $p = 0.95$). Similarly, input resistance (R_{in}), membrane capacitance (C_m) and resting membrane potential (V_m) were not significantly affected by expression of $\text{Ca}_v2.1[\text{Efa}]$ or $\text{Ca}_v2.1[\text{EFb}]$ (R_{in} (in $\text{M}\Omega$): 499 ± 38 ; 495 ± 25 ; 413 ± 20 ; $p = 0.39$; C_m (in pF): 219 ± 9 ; 200 ± 10 ; 229 ± 8 ; $p = 0.49$; V_m (in mV): -63.9 ± 1.4 ; -64.2 ± 1.2 ; -63.6 ± 0.8 ; $p = 0.97$; $n = 14, 17$ and 31 for Efa, EFb and Control, respectively).

Electrophysiology and optogenetics in acute brain slices

All experiments were performed in accordance with EU and Italian regulations. Fifteen-24 days post-injection, male Sprague Dawley rats were decapitated under deep isoflurane anesthesia and sagittal slices of the hippocampal formation ($350 \mu\text{m}$ thick) were prepared with a Vibratome (Leica VT1200S) under low-light conditions. Slices were maintained submerged in gassed (95% O_2 , 5% CO_2) aCSF containing (in mM): 123 NaCl, 1.25 KCl, 1.25 KH_2PO_4 , 1.5 MgCl_2 , 1 CaCl_2 , 25 NaHCO_3 , 2 NaPyruvate and 18 glucose (osmolarity adjusted to 300 mOsm). After recovering for 30 min at 37°C and for ≥ 30 min at room temperature, slices were transferred to a submerged recording chamber and superfused at 2 ml/min with the same aCSF used for recovery supplemented with 1.5 mM CaCl_2 (total Ca^{2+} : 2.5 mM). Tight-seal whole-cell recordings were obtained from pyramidal neurons in the proximal to medial tract of the CA1 region under visual control using infrared illumination. Patch electrodes (5–6 $\text{M}\Omega$) were filled with an intracellular solution containing (in mM): 110 K-gluconate, 22 KCl, 5 NaCl, 0.5 EGTA, 3 MgCl_2 , 4 Mg-ATP, 0.5 $\text{Na}_3\text{-GTP}$, 20 $\text{K}_2\text{-creatine phosphate}$, 10 HEPES-KOH (pH 7.28; osmolarity adjusted to 290 mOsm). Experiments were performed in the presence of 10 μM Bicuculline, to block inhibitory synaptic transmission, and started after ~ 10 min following breakthrough. EPSCs were evoked with a 473 nm Blue Laser (MBL-III-473 Solid State 1–200mW; Information Unlimited) coupled via a 20x 0.40 N.A. objective to an optical fiber (250 μm in diameter) positioned directly on CA3 somata. Care was taken to shine light away from the Schaffer collaterals, so to avoid direct depolarization of the axons. Whenever applied (in 20 out of 39 recordings), TTX always completely blocked EPSCs (**figure S5B, C**), showing that optically evoked EPSCs are AP-driven. Stimulation length was set to 2 ms and inter-pulse to 50 ms because the ultrafast channelrhodopsin ChETA responds most reliably at these stimulations without displaying extra-spikes (Gunaydin et al., 2010). Stimulation strength (1–3 mW at fiber exit) was adjusted with neutral density filters to yield small, but clearly detectable, EPSCs (< 30 pA peak amplitude at -70 mV; **figure 6D, S5D, E**). Using these conditions, optical stimulation every 20 sec reliably produced stable EPSCs for the time of the experiment (37 minutes; **figure S5B**). To prevent unspecific binding on glass and plastic surfaces, ω -conotoxin-GVIA (1 μM) was applied in the presence of cytochrome C (30 $\mu\text{g/ml}$). Nineteen out of 39 experiments were terminated with NBQX application (10 μM), which always completely blocked EPSCs (**figure S5B, C**), showing that optically-evoked EPSCs are mediated by AMPARs. Data were low-pass filtered at 5 kHz and acquired at 50 kHz with EPC10 amplifier (HEKA) and PatchMaster software (HEKA). Analysis was performed offline using Clampfit 10.1 (Molecular Devices) and Igor Pro 6.03 (Wavemetrics Inc.). Series resistances were always $\leq 25 \text{ M}\Omega$, not significantly different between experimental groups, and left uncompensated. Cells were rejected if series resistance changed by more than 20% during the course of the experiment. Twenty-four traces during baseline and the last 24 traces during ω -conotoxin-GVIA application were averaged before calculating PPR (Kim and Alger, 2001).

Synaptic latency, measured from the end of the light pulse to 5% of the EPSC amplitude (Boudkkazi et al., 2007), was not modified by $\text{Ca}_v2.1[\text{Efa}]$ or $\text{Ca}_v2.1[\text{EFb}]$ knockdown (miR Control: 6.67 ± 0.25 ms; miR Efa1: 6.71 ± 0.25 ms; miR Efa3: 6.71 ± 0.18 ms; miR EFb2: 6.59 ± 0.17 ms; $p = 0.99$). Similarly, input resistance (R_{in}), membrane capacitance (C_m) and resting membrane potential (V_m) were not significantly different between experimental conditions (R_{in} (in $\text{M}\Omega$): 204 ± 11 ; 184 ± 6 ; 202 ± 4 ; 178 ± 4 ; $p = 0.53$; C_m (in pF): 501 ± 21 ; 449 ± 23 ; 512 ± 16 ;

424 ± 20; p = 0.36; V_m (in mV): -60.2 ± 0.6; -58.8 ± 0.7; -57.9 ± 0.6; -60.6 ± 0.7; p = 0.37; n = 12, 9, 9 and 11 for miR Control, miR EFa1, miR EFa3 and miR Efb2, respectively).

Presynaptic Ca²⁺ imaging with SyGCaMP3 and SyGCaMP6s

Imaging was performed in rat primary cultures at room temperature in aCSF containing (in mM): 140 NaCl, 2.5 KCl, 2.2 CaCl₂, 1.5 MgCl₂, 10 D-glucose, 0.01 CNQX, 0.05 D-APV and 10 HEPES-NaOH (pH 7.38; osmolarity adjusted to 290 mOsm). For experiments in **figure S3A-C**, we selected SyGCaMP3 (K_D=345-405 nM; Hill coefficient = 2.10-2.54 for GCaMP3) (Akerboom et al., 2012; Chen et al., 2013) as Ca²⁺ reporter because it displayed the lowest cooperative behavior amongst the Ca²⁺ indicators we tested (GCaMP3, GCaMP5g and GCaMP6s). Cultures were co-transfected with SyGCaMP3, the auxiliary subunit β4 and Ca_v2.1[EFa] or Ca_v2.1[EFb] in a 1:1:1 DNA ratio 3-5 days prior to experiments, and measured at 13-15 DIV.

For experiments in **figure S4D-F**, we selected SyGCaMP6s (K_D=144 nM; Hill coefficient = 2.90 for GCaMP6s) (Chen et al., 2013) as Ca²⁺ reporter because, despite its highly non-linear behavior, it was the most sensitive amongst the Ca²⁺ indicators we tested, enabling us to detect presynaptic Ca²⁺ transients also after partial blockade of Ca²⁺ entry. Cultures were co-transfected with SyGCaMP6s and the required miR construct in a 1:1 DNA ratio 6-8 days prior to experiments, and measured at 16-18 DIV. Experiments were performed in the presence of ω-conotoxin GVIA (1 μM) to block N-type Ca²⁺ channels. Because P/Q-type and N-type Ca²⁺ channels give the largest contribution to synaptic transmission at hippocampal synapses (Reid et al., 1998; Scholz and Miller, 1995), this experimental configuration enabled us to investigate the contribution of P/Q-type channel splice isoforms to presynaptic Ca²⁺ in relative isolation.

Boutons were imaged using a cooled charge-coupled device (CCD) camera (ORCA-R2, Hamamatsu) mounted on an inverted microscope (DMI6000B, Leica) with a 40x, 1.25 NA oil immersion objective. A 200W metal halide lamp (Lumen200Pro, Prior Scientific) and a filter set comprising a BP 470/40 nm excitation filter, a 500 nm dichroic mirror and a BP 525/50 emission filter (Leica) were used for illumination. Images were captured at 15.3 Hz with 50 ms integration times at a depth of 8 bits. APs were evoked by field stimulation (60 V, 1 ms pulses; Isolated Pulse Stimulator, A-M systems) using a custom-made chamber with two parallel platinum wires 6 mm apart. Trains of APs were delivered at a frequency of 40 Hz every 18 s.

Images were analyzed in ImageJ (<http://rsb.info.nih.gov/ij>) with the plugin Time Series Analyzer V2.0 (<http://rsb.info.nih.gov/ij/plugins/time-series.html>) and with customized routines in Igor Pro 6.03. Regions of interest (ROIs) with a diameter of 3.2 μm were positioned on all boutons responding to six APs for SyGCaMP3 and to 20 APs for SyGCaMP6s with a signal above two SD of the background noise. The intensity of a twin ROI positioned within 10 μm from the first was used to subtract the local background noise. Signals were quantified as ΔF/F₀, where ΔF=F-F₀, with F₀ measured over 1 s period prior to stimulation.

Presynaptic Ca²⁺ imaging with Fluo-4

Imaging was performed at room temperature in aCSF containing (in mM): 125 NaCl, 2.5 KCl, 1 CaCl₂, 3 MgCl₂, 20 D-glucose, 0.01 CNQX, 0.05 D-APV and 25 HEPES-NaOH (pH 7.40; osmolarity adjusted to 310 mOsm) as previously described (Ermolyuk et al., 2012). Briefly, neurons were loaded via a whole-cell patch pipette with a mixture of the high affinity Ca²⁺ fluorescence dye Fluo-4 (200 μM, Invitrogen) and the morphological tracer Alexa 568 (200 μM, Invitrogen), added to an intracellular solution containing (in mM) 135 K-methanesulfonate, 10 HEPES, 10 Na-Phosphocreatine, 4 MgCl₂, 4 Na₂-ATP, 0.4 Na₃-GTP. Five minutes after breaking in, the patch pipette was slowly withdrawn to minimize cytosol dialysis. Ca²⁺ fluorescence recordings were started at least 30 min after retracting the patch pipette to allow the fluorophores to equilibrate throughout the neuron. APs were evoked by field stimulation via platinum bath electrodes separated by 1 cm (12.5 – 15 V, 1 ms pulses). Fluorescence transients in identified boutons were recorded in response to alternating single and double pulse (at 40 Hz) stimulation in fast line-scan mode (~ 500 Hz, 5 trials averaged for analysis) using an inverted LSM 510 confocal microscope (Zeiss) equipped with a 63x (1.4 NA) oil immersion objective. To minimize optical artifacts, the Fluo-4 fluorescence was normalized to the average Alexa 568 fluorescence determined in each sweep (G(t)/R ratio). The amplitude of the Ca²⁺ influx during the first AP (ΔG₁/R) was calculated by subtracting the resting fluorescence (G_{rest}/R) from the fluorescence signal integrated over a 10 ms window immediately after the first AP (G_{AP}/R). The amplitude of the Ca²⁺ influx during the second AP (ΔG₂/R) was calculated in a similar manner, after subtracting the Ca²⁺ fluorescence to a single AP from the Ca²⁺ fluorescence to a pair of APs (**figure S3F**).

Fluo-4 provides a linear readout of AP-evoked presynaptic Ca²⁺ influx if the ΔG/G_{max} ratio is below 0.6 (where G_{max} is the maximal fluorescence of the saturated Fluo-4 signal determined with 100 APs delivered at 100 Hz (Ermolyuk et al., 2012)). To meet this requirement, we determined that the ratio G_{max}/R was always below two in our experimental conditions, and excluded from the analysis all the boutons where the response to the first AP (ΔG₁/R) was higher than 0.6 (this corresponding to a cutout of ΔG/G_{max} ≤ 0.3 for a single AP). We also excluded from the analysis all boutons where ΔG₁/R was lower than 0.1 because a poor signal to noise ratio in these boutons precluded us from reliably determining ΔG₂/ΔG₁.

Imaging of vesicle cycling with synaptophysin-pHluorin

Synaptophysin-pHluorin (SypHy) was imaged in aCSF containing (in mM): 140 NaCl, 2.5 KCl, 2.2 CaCl₂, 1.5

MgCl₂, 13 D-glucose, 0.01 CNQX, 0.05 D-APV and 12 HEPES-NaOH (pH 7.38; osmolarity adjusted to 320 mOsm). Alkalization of the entire vesicle pool was achieved with aCSF differing from the above for the presence of NH₄Cl (50 mM) and for a reduced content of NaCl (60 mM). For experiments in **figure 3A, B**, cultures were co-transfected with SypHy, the auxiliary subunit β4 and Ca_v2.1[EFa] or Ca_v2.1[EFb] in a 1:1:1 DNA ratio 3-4 days prior to experiments, and measured at 13-14 DIV. For experiments in **figure 5**, cultures were co-transfected with SypHy and the required miR construct in a 1:1 DNA ratio 6-8 days prior to experiments, and measured at 16-18 DIV. Under basal conditions, SypHy responses in the knockdown experiments were considerable larger than those in the over-expression experiments (compare figure 5B with 3B). This is because of differences in culture age, time of expression and amount of SypHy DNA used for transfection in the two sets of experiments (A.T. and L.A.C., unpublished observations). SypHy responses were stable and reproducible for the time period of the experiment (16 min). EGTA-AM (200 μM) was loaded for 90 s, followed by 10 min wash (Hoppa et al., 2012). In control experiments, application of DMSO at the same final concentration used to dissolve EGTA-AM (0.1%) did not affect SypHy responses (n=3, 3 and 2 independent experiments for Ca_v2.1[EFa], Ca_v2.1[EFb] and Control, respectively). Images were captured at 2 Hz with 100 ms integration times and analyzed offline in ImageJ as for SyGCaMP experiments. Signals were background subtracted and quantified as $\Delta F = F - F_0$, where F_0 was measured over a 5 s period prior to stimulation.

Synaptotagmin antibody live uptake and confocal microscopy

Imaging was performed as previously described (Cingolani et al., 2008). Briefly, primary hippocampal cultures were transfected at 10 DIV and fixed at 14 and 17-18 DIV for the over-expression and knockdown experiments, respectively. Fixation was performed with 4% paraformaldehyde/4% sucrose (12 min), permeabilization with methanol (-20°C; 10 min on ice) followed by 0.2% Triton X-100 (10 min) (Liao et al., 1999) and blocking with 4% NGS/0.1% BSA (30 min). The following primary antibodies were used: chicken anti-GFP (1:1000; Cat. No. 13970, Abcam), rabbit anti-Ca_v2.1 (1:1000; Cat. No. 152203, Synaptic Systems), rabbit anti-Ca_v2.1 (1: 250; Cat. No. 152103, Synaptic Systems; this antibody was used for experiments in figure S2A-B, as it is specific for rodent Ca_v2.1 (Schneider et al., 2015), rabbit anti Ca_v2.2 (1:100; Cat. No. ACC-002, Alomone Labs), mouse anti-RFP (1:2000; Cat. No. 200-301-379, tebu-bio) and guinea pig anti-bassoon (1:500; Cat. No. 141004, Synaptic Systems). Secondary antibodies were Alexa488 goat anti-chicken, Alexa488 goat anti-rabbit, Alexa568 goat anti-rabbit, Alexa568 goat anti-mouse and Alexa647 goat anti-guinea pig IgGs (1:1000 in all cases; Cat. No. A11039, A11034, A11036, A11031 and A21450, respectively, Invitrogen). Confocal stacks were acquired at 200 Hz with a Leica SP8 using a 63x oil immersion objective (NA 1.40), 1.2x digital zoom, 0.15 μm pixel size, 1 AU pinhole, 0.3 μm between optical sections, with a sequential line-scan mode and 3x scan averaging. For all experimental conditions compared, the same settings for laser intensity, offset and PMT gain were used.

Confocal images were analyzed using ImageJ. Each single stack was filtered using a Gaussian filter (radius: 0.5 pixels), and the maximal fluorescence intensities of in-focus stacks were Z-projected. Analysis of fluorescence intensity was performed on axonal ROIs (2-3 per image) of 50-150 μm in lengths, manually selected blind to the experimental condition. The ROIs were automatically thresholded using a fixed value (30 a.u.) for Ca_v2.1 over-expressed constructs, mode plus three standard deviations of the gray scale histogram for endogenous Ca_v2.1, mode plus half standard deviation of the gray scale histogram for TdTomato and the Robust Automatic Threshold Selection plugin for bassoon. Colocalization between bassoon and Ca_v2.1 was estimated for the thresholded ROIs with the Coloc2 plugin using the Manders' coefficients ($M_A = \sum_i A_{i,coloc} / \sum_i A_i$, where $\sum_i A_i$ is the sum of intensities of all pixels above threshold for channel A and $\sum_i A_{i,coloc}$ is calculated as $\sum_i A_i$ but only for pixels where also the second channel B is above threshold).

For the synaptotagmin antibody live uptake, we treated cultures with CNQX (20 μM) and D-APV (100 μM) 24 hours prior to experiment. This protocol is very effective in inducing presynaptic homeostatic plasticity, including up-scaling of presynaptic P/Q-type channels (Lazarevic et al., 2011), while differentially affecting Ca_v2.1 splice isoform expression at the mRNA level (**figure 7A**). We blocked N-type Ca²⁺ channels with ω-conotoxin GVIA (1 μM) starting 30 min prior to uptake in order to investigate the contribution of P/Q-type channel splice isoforms to vesicle release in relative isolation (Reid et al., 1998; Scholz and Miller, 1995). A subset of coverslips treated also with ω-agatoxin TK (300 nM) for the same time period served as negative control. Neurons were rinsed twice in aCSF containing (in mM): 140 NaCl, 5 KCl, 2.2 CaCl₂, 1.5 MgCl₂, 15 D-glucose, 0.01 CNQX, 0.05 D-APV, 0.001 ω-conotoxin GVIA and 12 HEPES-NaOH, with or without 0.0003 ω-agatoxin TK (pH 7.38; osmolarity adjusted to 320 mOsm), before performing the synaptotagmin antibody live uptake in the same aCSF for 12 min at 37°C with a mouse antibody against the luminal domain of synaptotagmin 1 (1:200; Cat. No. 105311, Synaptic Systems). In initial cell-attached and whole-cell electrophysiological recordings, we established that these conditions support spontaneous neuronal firing at low rate (≤10 Hz), thus being suitable for detecting activity-dependent changes in presynaptic activity (Lazarevic et al., 2011). After three washes in the same aCSF, neurons were fixed and processed for immunofluorescence as above. The following primary antibodies were used: chicken anti-RFP (1:500; Cat. No. 600-901-379, tebu-bio) and rabbit anti-Ca_v2.1 (1:1000; Cat. No. 152203, Synaptic Systems). Secondary antibodies were Alexa488-, Alexa568- and Alexa647-conjugated goat anti-mouse, anti-chicken and anti-rabbit (1:1000 in all cases; Cat. No. A11029, A11041 and A21245, respectively, Invitrogen).

Confocal images were acquired and analyzed as above with the following modifications: active boutons within

TdTomato-positive axons were selected blind to the experimental conditions in the synaptotagmin channel using the ImageJ plugin Time Series Analyzer V3.0 (circular ROIs, \varnothing 1.2 μ m). The synaptotagmin and Ca_v2.1 signals within each ROI were then automatically thresholded using a fixed value (22 a.u.) for all conditions.

Statistical analysis

Unless otherwise stated, statistical differences were assessed using paired and unpaired two-tailed Student's t-test, and the one-way analysis of variance test followed by the Tukey-Kramer post-test, as required. The analysis of covariance was used for figures 1E, 3D, 6E and S5F; the Kruskal-Wallis test followed by the Dunn's multiple comparison post-test for figure 1G; the one-way analysis of variance test followed by the linear trend post-test to analyze the correlation between synaptotagmin uptake and Ca_v2.1 signal in figure S6B (Prism 5, GraphPad Software Inc.); the Kolmogorov-Smirnov test for figure S4F (http://www.physics.csbsju.edu/stats/KS-test.n.plot_form.html). Unless otherwise stated, average data are expressed as mean+SEM.

Supplemental references

- Akerboom, J., Chen, T.W., Wardill, T.J., Tian, L., Marvin, J.S., Mutlu, S., Calderon, N.C., Esposito, F., Borghuis, B.G., Sun, X.R., *et al.* (2012). Optimization of a GCaMP calcium indicator for neural activity imaging. *J Neurosci* *32*, 13819-13840.
- Boudkkazi, S., Carlier, E., Ankri, N., Caillard, O., Giraud, P., Fronzaroli-Molinieres, L., and Debanne, D. (2007). Release-dependent variations in synaptic latency: a putative code for short- and long-term synaptic dynamics. *Neuron* *56*, 1048-1060.
- Bourinet, E., Soong, T.W., Sutton, K., Slaymaker, S., Mathews, E., Monteil, A., Zamponi, G.W., Nargeot, J., and Snutch, T.P. (1999). Splicing of alpha 1A subunit gene generates phenotypic variants of P- and Q-type calcium channels. *Nat Neurosci* *2*, 407-415.
- Cao, Y.Q., Piedras-Renteria, E.S., Smith, G.B., Chen, G., Harata, N.C., and Tsien, R.W. (2004). Presynaptic Ca₂⁺ channels compete for channel type-preferring slots in altered neurotransmission arising from Ca₂⁺ channelopathy. *Neuron* *43*, 387-400.
- Cao, Y.Q., and Tsien, R.W. (2010). Different relationship of N- and P/Q-type Ca₂⁺ channels to channel-interacting slots in controlling neurotransmission at cultured hippocampal synapses. *J Neurosci* *30*, 4536-4546.
- Chaudhuri, D., Chang, S.Y., DeMaria, C.D., Alvania, R.S., Soong, T.W., and Yue, D.T. (2004). Alternative splicing as a molecular switch for Ca₂⁺/calmodulin-dependent facilitation of P/Q-type Ca₂⁺ channels. *J Neurosci* *24*, 6334-6342.
- Chen, T.W., Wardill, T.J., Sun, Y., Pulver, S.R., Renninger, S.L., Baohan, A., Schreiter, E.R., Kerr, R.A., Orger, M.B., Jayaraman, V., *et al.* (2013). Ultrasensitive fluorescent proteins for imaging neuronal activity. *Nature* *499*, 295-300.
- Cingolani, L.A., and Goda, Y. (2008). Differential involvement of beta3 integrin in pre- and postsynaptic forms of adaptation to chronic activity deprivation. *Neuron Glia Biol* *4*, 179-187.
- Cingolani, L.A., Thalhammer, A., Yu, L.M., Catalano, M., Ramos, T., Colicos, M.A., and Goda, Y. (2008). Activity-dependent regulation of synaptic AMPA receptor composition and abundance by beta3 integrins. *Neuron* *58*, 749-762.
- Deidda, G., Parrini, M., Naskar, S., Bozarth, I.F., Contestabile, A., and Cancedda, L. (2015). Reversing excitatory GABAAR signaling restores synaptic plasticity and memory in a mouse model of Down syndrome. *Nat Med* *21*, 318-326.
- Dreosti, E., Odermatt, B., Dorostkar, M.M., and Lagnado, L. (2009). A genetically encoded reporter of synaptic activity in vivo. *Nat Methods* *6*, 883-889.
- Ermolyuk, Y.S., Alder, F.G., Henneberger, C., Rusakov, D.A., Kullmann, D.M., and Volynski, K.E. (2012). Independent regulation of Basal neurotransmitter release efficacy by variable Ca(2)⁺ influx and bouton size at small central synapses. *PLoS Biol* *10*, e1001396.
- Gunaydin, L.A., Yizhar, O., Berndt, A., Sohal, V.S., Deisseroth, K., and Hegemann, P. (2010). Ultrafast optogenetic control. *Nat Neurosci* *13*, 387-392.
- Hoppa, M.B., Lana, B., Margas, W., Dolphin, A.C., and Ryan, T.A. (2012). alpha2delta expression sets presynaptic calcium channel abundance and release probability. *Nature* *486*, 122-125.

- Kim, J., and Alger, B.E. (2001). Random response fluctuations lead to spurious paired-pulse facilitation. *J Neurosci* *21*, 9608-9618.
- Lazarevic, V., Schone, C., Heine, M., Gundelfinger, E.D., and Fejtova, A. (2011). Extensive remodeling of the presynaptic cytomatrix upon homeostatic adaptation to network activity silencing. *J Neurosci* *31*, 10189-10200.
- Li, H., Foss, S.M., Dobryy, Y.L., Park, C.K., Hires, S.A., Shaner, N.C., Tsien, R.Y., Osborne, L.C., and Voglmaier, S.M. (2011). Concurrent imaging of synaptic vesicle recycling and calcium dynamics. *Front Mol Neurosci* *4*, 34.
- Liao, D., Zhang, X., O'Brien, R., Ehlers, M.D., and Huganir, R.L. (1999). Regulation of morphological postsynaptic silent synapses in developing hippocampal neurons. *Nat Neurosci* *2*, 37-43.
- McClure, C., Cole, K.L., Wulff, P., Klugmann, M., and Murray, A.J. (2011). Production and titering of recombinant adeno-associated viral vectors. *J Vis Exp*, e3348.
- Niwa, H., Yamamura, K., and Miyazaki, J. (1991). Efficient selection for high-expression transfectants with a novel eukaryotic vector. *Gene* *108*, 193-199.
- Qian, J., and Noebels, J.L. (2000). Presynaptic Ca(2+) influx at a mouse central synapse with Ca(2+) channel subunit mutations. *J Neurosci* *20*, 163-170.
- Reid, C.A., Bekkers, J.M., and Clements, J.D. (1998). N- and P/Q-type Ca²⁺ channels mediate transmitter release with a similar cooperativity at rat hippocampal autapses. *J Neurosci* *18*, 2849-2855.
- Saunders, A., Johnson, C.A., and Sabatini, B.L. (2012). Novel recombinant adeno-associated viruses for Cre activated and inactivated transgene expression in neurons. *Front Neural Circuits* *6*, 47.
- Scheuber, A., Miles, R., and Poncer, J.C. (2004). Presynaptic Cav2.1 and Cav2.2 differentially influence release dynamics at hippocampal excitatory synapses. *J Neurosci* *24*, 10402-10409.
- Schneider, R., Hosy, E., Kohl, J., Klueva, J., Choquet, D., Thomas, U., Voigt, A., and Heine, M. (2015). Mobility of calcium channels in the presynaptic membrane. *Neuron* *86*, 672-679.
- Scholz, K.P., and Miller, R.J. (1995). Developmental changes in presynaptic calcium channels coupled to glutamate release in cultured rat hippocampal neurons. *J Neurosci* *15*, 4612-4617.
- Silver, R.A. (2003). Estimation of nonuniform quantal parameters with multiple-probability fluctuation analysis: theory, application and limitations. *J Neurosci Methods* *130*, 127-141.
- Thalhammer, A., and Cingolani, L.A. (2014). Cell adhesion and homeostatic synaptic plasticity. *Neuropharmacology* *78*, 23-30.
- Vandesompele, J., De Preter, K., Pattyn, F., Poppe, B., Van Roy, N., De Paepe, A., and Speleman, F. (2002). Accurate normalization of real-time quantitative RT-PCR data by geometric averaging of multiple internal control genes. *Genome Biol* *3*, RESEARCH0034.
- Wu, L.G., and Saggau, P. (1994). Pharmacological identification of two types of presynaptic voltage-dependent calcium channels at CA3-CA1 synapses of the hippocampus. *J Neurosci* *14*, 5613-5622.